



Contents lists available at ScienceDirect

International Journal of Adhesion and Adhesives

journal homepage: <http://www.elsevier.com/locate/ijadhadh>

PLGA nanoparticles loaded with quaternary ammonium silane and riboflavin for potential applications in adhesive dentistry

Umer Daood^{a,1}, Meera Priyadarshini Balasankar^{b,1}, Marrwa A. Ibrahim^c,
Mallikarjuna Rao Pichika^d, Kit-Kay Mak^d, Amr S. Fawzy^{e,*}

^a Clinical Dentistry, Restorative Division, Faculty of Dentistry, International Medical University Kuala Lumpur, 126, Jalan Jalil Perkasa 19, Bukit Jalil, 57000, Bukit Jalil, Wilayah Persekutuan Kuala Lumpur, Malaysia

^b National University of Singapore, 1E Kent Ridge Road, Singapore, 119228

^c School of Human Sciences, University of Western Australia, WA, 6009, Australia

^d Department of Pharmaceutical Chemistry, School of Pharmacy, International Medical University Kuala Lumpur, 126, Jalan Jalil Perkasa 19, Bukit Jalil, 57000, Bukit Jalil, Wilayah Persekutuan Kuala Lumpur, Malaysia

^e UWA Dental School, University of Western Australia, WA, 6009, Australia

ARTICLE INFO

Keywords:

k21
Quaternary ammonium silane
Bonding
Drug-loaded nanoparticles
Dental biofilm

ABSTRACT

Aim: Novel k21 PLGA nanoparticles (nano-PLGA-RF/VE-TPGS_{0.50}:k21) with synergistic effect of VE-TPGS with riboflavin-5-phosphate solution were used to analyze structural integrity, chemical interactions, antimicrobial resistance, mechanical properties as a delivery tool to acid-demineralized dentine-substrates.

Materials and methods: Synthesized spherical nano-PLGA:RF/VE-TPGS_{0.50}:k21 were assessed for drug-encapsulation and release, antibacterial-profile, MTT, molecular simulation for MMP-2 and MMP-9 and Raman spectroscopy.

Results: k21 favoured increase in colloidal-size with positive zeta potential. Bands indicated k21 entrapment as nanoparticles were confined inside tubules with no effect on μ TBS. XP-GScores were -2.383 and -4.383 for MMP-2 and -9. HYP liberation recorded with collagenase degradation resistance in nano-PLGA:RF/VE-TPGS_{0.50}:k21 specimens.

Conclusion: Nano-PLGA:RF/VE-TPGS_{0.50}:k21 specimens exhibited superior antibacterial/antibiofilm effects against cariogenic biofilms after bonding-resins infiltration without adversely affecting bond strength.

1. Introduction

Oral cavity harbors a conducive environment for heterogeneous microbial communities present either as free-floating planktons and/or biofilms [1]. Biomaterials used for restoration of tooth function are biofilm-prone due to increased number of sites on their hydrophobic rough surfaces [2,3]. *Streptococcus mutans* is known to initiate tooth decay that progresses into an established lesion [4]. The central part of biofilm matrix has reduced oxygen and an anaerobic environment and is neutral or polyanionic due to presence of uronic acids or ketal-linked pyruvates [5]. Therefore, bonding to carious dentine produces inferior results irrespective of adhesive system used [6] due to wetness, tubular-occlusion, loss of minerals and degradation of bonded interface by matrix-metalloproteinases [7]. Hence, new strategies are required to

intercept caries with new antimicrobial agents [8].

Quaternary ammonium silane (QAS/k21; KHG FiteBac® Technology, Marietta, GA, USA) is an organic contact-killing antibacterial agent that possesses broad-spectrum antimicrobial activities with low cytotoxicity [9,10]. The $-C_{18}H_{37}$ lipophilic-alkyl chain within k21 molecule penetrates bacterial cell membrane resulting in autolysis due to an osmotic imbalance [11]. The compound has been synthesized via sol-gel process using cationic 3-(trimethoxysilyl)-propyldimethyloctadecyl ammonium chloride (SiQAC; C₂₆H₅₈ClNO₃Si; CAS Number 27668-52-6) [12] and tetraethoxysilane (TEOS) via sol-gel reaction to produce a host of molecules with different molecular weights that are collectively code-named k21 (CAS Registry Number 1566577-36-3; IUPAC name: 1-octadecanaminium, N,N'-[[[3-bis [[3-(dimethyl octadecylammonio) propyl] dihydroxysilyl]oxy]-1,1,5,5-tetrahydroxy-1,5-trisiloxanediyl]di-3,

* Corresponding author. 17 Monash Avenue, Nedlands, WA, 6009, Australia.

E-mail address: amr.fawzy@uwa.edu.au (A.S. Fawzy).

¹ Authors have contributed equally.

<https://doi.org/10.1016/j.ijadhadh.2020.102797>

1-propanediyl] bis [*N,N*-dimethyl] chloride (1:4) [13]. Presence of TEOS enables a three-dimensional network comprised of silicate with condensation of tetra and tri-ethoxysilane with remaining silanol groups [14] on demineralized dentine. This three-dimensional organically modified silicate is produced by condensation of additional tetraethoxy and triethoxy molecules with remnant silanol groups within the k21 molecule. The three-dimensional network to be formed once condensation is brought to completion within the dentinal substrate.

In order to reduce limiting factor of delivery and bioavailability, various approaches such as emulsions, polymeric-micelles, proliposomes and PLGA-PEG based nanocarriers were adopted by researchers [15,16]. Poly (lactic-co-glycolic acid) (PLGA) is an extensively investigated polymer approved by the US Food and Drug Administration (FDA) for medical applications [17]. PLGA nanoparticles have proved to be a potential drug delivery system [18] and is one of the best characterized biodegradable copolymers decomposing into non-toxic products (CO₂ and H₂O) that are eliminated from the body. PLGA is produced by ring-opening copolymerization of LA and GA having low water solubility under physiological conditions [19]. This pioneer study features the use of k21-loaded PLGA-nanoparticles in combination with dentine-bonding resins, used to bond restorative resin-based composites to dentine, and the effect on dentin-related cariogenic *S. mutans* biofilms. Accordingly, we successfully delivered nanoparticles (proanthocyanidins-loaded) to acid-demineralized dentine-substrates through dentinal tubules as a novel route for drug-delivery to dentine [20].

Resin-dentine hybrid layer is prone to degradation due to host-derived proteinases [21]. Suboptimal infiltration of denuded collagen fibrils is very common, especially as observed with etch-and-rinse adhesives [22] and self-etch adhesives [23]. Collagen crosslinkers have been recently investigated to improve collagen degradation and inactivate collagenolytic enzymes [24]. In our previous work, d-alpha-tocopheryl poly (ethyleneglycol)-1000-succinate (VE-TPGS) was used as a permeation enhancer for improving the uptake of riboflavin [25]. Vitamin-E TPGS is a non-surfactant transporting riboflavin through barriers [26] protecting free-radical damage associated with reactive oxygen species generation [27]. In current study, synergistic effect of VE-TPGS with riboflavin-5-phosphate solution (at RF/VE-TPGS (w/w) ratios of 0.125/0.50 (RF/VE-TPGS_{0.50}) coupled with different concentrations of k21 within PLGA nanoparticle was investigated. Use of quaternary ammonium silane (k21) had preserved dentine bond strength and enhanced bond durability. The compound was not cytotoxic and showed both antibacterial as well as anti-protease properties [9,10]. Our interest was in collagen structural integrity and conformational stability, chemical interactions, antimicrobial resistance, mechanical properties, and endogenous proteases inhibition. In this regard, the aim is to fabricate PLGA-VE/TPGS loaded with different concentrations of k21 nanoparticles, which were then characterized for their morphological and physicochemical characteristics; drug-loading; drug-release; *in vitro* cytotoxicity, antibacterial/antibiofilm potential and extensive chemical and simulation characterization. In addition, these nanoparticles were infiltrated to demineralized dentin-substrates under simulated pulpal hydrostatic-pressure, followed by the application of a two-step etch-and-rinse (E&R) dentine-bonding resins. Resin-dentin bonded specimens that were treated with these nanoparticles were tested for nanoparticles delivery inside dentinal tubules, resin-dentin interfacial morphology, micro-tensile bond strength (μ TBS) after storage for 12 months in distilled water at 37 °C and for their *anti*-biofilm potential using *S. mutans* cultured over the resin-infiltrated dentine surfaces.

2. Materials and Methods

Experimental versions of k21 cavity disinfectants were generously provided by KHG *FiteBac*®-Technology. Poly (lactic-co-glycolic acid) (PLGA; 75:25; Mw~66,000–107,000), dichloromethane, polyvinyl alcohol (PVA), distilled water, potassium bromide (FTIR grade),

phosphate buffered saline (PBS), crystal violet solution, NaCl, phenol, glacial acetic acid, H₂SO₄ and Riboflavin were obtained from Sigma Aldrich. Adper Scotchbond™ Etchant, Adper™ Single bond 2 two-step E&R system, resin-composite (Filtek Z350, XTA3.5) and micro-brushes were purchased from 3M-ESPE (St. Paul, MN, USA). Riboflavin/RF (–) ≥98% (CAS Number 83-88-5), Molecular Weight 382.35 was purchased from (Thermo Fisher Scientific Nicolet, Waltham, MA, USA) in powdered form. Human molars (*n* = 90; aged 21–34 years) were collected after patient's informed consent (protocol approved by Institutional Review Board at University of Western Australia [PG10402012] NUS [Oral Health Seed Grant R221000078733] and International Medical University [425/2018]) and stored in a solution of sodium azide (0.2%) at 4 °C.

2.1. Synthesis of nanoparticles

Riboflavin phosphate buffer (IGP, potassium phosphate buffer 0.50, pH 7.0; ThermoFisher, Kuala Lumpur, Malaysia), PLGA (50 mg), and acetone (10 mL) was used to disperse inside vitamin E d-alpha-tocopheryl polyethylene glycol 1000 succinate riboflavin (RF/VE-TPGS) solution (20 mL, 0.03% w/v; Eastman Chemicals, New York, USA) at w/w ratios of 0.125/0.50 (RF/VE-TPGS_{0.50}) in a single individual mix using probesonication (Soniprep 150, Fisons, Sussex, England) (25 °C, 25% amplitude) for 15 min at room temperature. Riboflavin-5-phosphate (Sigma-Aldrich) was dissolved in distilled water inside light proof test tubes to obtain 0.125% RF formulations. Next, VE-TPGS was added directly to RF-solution, at RF/VE-TPGS (w/w) ratio of 0.125/0.50 (RF/VE-TPGS_{0.50}).

The mixture was left undisturbed for 10 h and the solvent allowed to evaporate. The suspension obtained was filtered (Whatman filter paper 1) to remove any precipitate and later centrifuged at 18,000 rpm at 4 °C. The formed pellet was washed with distilled water and finally lyophilized (VirTis, USA) for 48 h to get a free-flowing powder. For k21 loading, about 100 mg of PLGA:RF/VE-TPGS_{0.50} was directly dissolved in dichloromethane at 50 °C. Upon obtaining a clear solution, different concentrations of k21 were added to the solution (~1 wt%, ~2 wt% and ~3 wt%). Under sonication, the above mixture was added dropwise to 2% aqueous solution of PVA. The mixture was then concentrated to 10 mL by slow evaporation under magnetic stirring for 3 h. A turbid appearance of solution indicated formation of Nano-PLGA:RF/VE-TPGS_{0.50}:k21 nanoparticles. Blank nanoparticles (nano-PLGA without k21 and RF/VE-TPGS_{0.50}) were also prepared. After preparation, nanoparticles were purified by centrifugation at 15,000 p.m. for 20 min.

2.2. Nanoparticles characterization

Nanoparticles were assessed by dynamic light scattering (DLS) (Malvern-Master sizer Nano ZS, UK) to measure the average size, zeta-potential (ζ), distribution profile and polydispersity index. Samples were diluted in distilled water [1:100 (wt/v)] and examined at 37 °C with a scattering angle of 90° (*n* = 10). Topographic details, morphology, size and shape of nano-PLGA:RF/VE-TPGS_{0.50} and PLGA:RF/VE-TPGS_{0.50}:k21 nanoparticles (different concentrations of k21 were deployed differently) were confirmed using transmission (TEM) (JEOL-JSM-1010, Japan) and scanning electron microscopy (SEM) (Joel FESEM JSM-6700 F, Japan). For TEM analysis, a drop of aqueous nanoparticle suspension (1:100 wt/v) was placed onto formvar/carbon-coated copper grids. Samples were evaporated by desiccation and then viewed (*n* = 5 per group). For SEM examination, dried nanoparticle powder was fixed on adhesive carbon tapes, gold sputter-coated (BAL-TEC, SCD 005 Sputter Coater, Scotia, NY, USA) and proceeded for imaging at an accelerating voltage of 10 kV (*n* = 5 per group).

Percentage (%) of k21 encapsulation and drug-loading of nanoparticles was measured directly by spectrophotometric analysis (UV-1700 Pharma Spec UV-Vis Spectrophotometer, Shimadzu, Japan) (*n* = 10 per group) at 289 nm by determining the amount of free non-

encapsulated k21 in the dispersion medium by centrifugation at 12,000 rpm at 25 °C for 15 min [28].

2.3. Drugs release profiles

In vitro release profile of RF [29] and k21 from nano-PLGA:RF/VE-TPGS_{0.50}:k21 at different ratios of k21 in PBS was studied up to 28 (for both) days. About 10 mg of nanoparticles was suspended in 15 mL of PBS (pH 7.4) at 37 °C under slow magnetic stirring. Samples were withdrawn at pre-estimated time intervals, centrifuged at 10,000 rpm for 15 min and analyzed by UV-spectrophotometer (UV-1700, Shimadzu, Japan) at 282 nm nano-PLGA/Blank were considered as control ($n = 7$ per group).

For riboflavin release, prepared nanoparticles were introduced in rotatory bottles consisting of 60 mL distilled water maintained at 46 rpm for 3 days at 37 °C. Later, 60 µL was taken after 25 min, diluted in distilled water and analyzed for riboflavin dissolution, repeating this step after each interval up to 28 days, using measurement of absorbance at 270 nm and a standard curve in distilled water.

2.4. Cytotoxicity analysis

In vitro cytotoxic activity of nano-PLGA:RF/VE-TPGS_{0.50} and nano-PLGA:RF/VE-TPGS_{0.50}:k21 nanoparticles was investigated using 3-(4,5-dimethyl-thiazol-2-yl)-2,5-diphenyl tetrazolium bromide (MTT) assay. Vybrant MTT Cell Proliferation Assay Kit (Thermo Fisher Scientific, Waltham, USA) was utilized according to protocol. Briefly, human mesenchymal stem cells (hMSCs) grown in mesenchymal stem cell growth medium (MSCGM™) (Lonza, Basel, Switzerland) were used. hMSCs were seeded in 96-well plates (10⁴ cells/well) and incubated at 37 °C in a 5% CO₂ ambience. Cells were cultured with different concentrations (0.5, 1 and 2 mg/mL) of nanoparticles, maintaining a treatment time of 48 h ($n = 7$). Cells in control group received no treatment. Upon treatment, cells were PBS-rinsed and incubated with 12 mM of MTT reagent stock solution for 4 h at 37 °C. Following another 3 h incubation with 100 µL of SDS-HCl solution to each well in a humidified, 5% CO₂ chamber at 37 °C, absorbance was measured at OD₅₇₀ and percentage (%) cell viability was calculated.

2.5. Bacterial strains and culture protocol

S. mutans (ATCC UA159) was revived from stored glycerol stock culture, sub-cultured in brain heart infusion (BHI) agar at 37 °C and incubated overnight. Single bacterial colonies obtained from these cultures were suspended in BHI medium for 24 h at 37 °C at 80-rpm and incubated for expansion. Concentration of cultures adjusted to $\sim 1.5 \times 10^8$ bacteria/mL at OD₆₀₀ were used for further bacterial experiments.

2.6. Anti-planktonic bacteria studies

Susceptibility of planktonic bacteria to nano-PLGA:RF/VE-TPGS_{0.50}, nano-PLGA:RF/VE-TPGS_{0.50}:1%k21, nano-PLGA:RF/VE-TPGS_{0.50}:2%k21 and nano-PLGA:RF/VE-TPGS_{0.50}:3%k21 were ascertained by inhibition zone method. Nanoparticles (1 mg/mL) impregnated sterile spherical filter paper discs were placed on bacteria swabbed BHI agar plates and incubated for 24 h at 37 °C. Diameters of growth inhibition zone were measured ($n = 5$ per group).

2.7. Antibiofilm studies

Biofilm quantification assay: Bacterial cultures were incubated in 24-well plates with 1 mg/mL of nano-PLGA:RF/VE-TPGS_{0.50}, nano-PLGA:RF/VE-TPGS_{0.50}:1%k21, nano-PLGA:RF/VE-TPGS_{0.50}:2%k21 and nano-PLGA:RF/VE-TPGS_{0.50}:3%k21 at 37 °C for 24 h without shaking to facilitate biofilm formation. Control cultures were devoid of nanoparticle treatment. Following incubation, cells were washed with

distilled water and stained with 0.4% (w/v) crystal violet solution for 10 min. Excess stain was removed using distilled water and 1 mL of 20% glacial acetic acid was added to solubilize the bound crystal violet. The absorbance of this extract was measured at OD₅₇₀ using microplate reader (Infinite 200, Tecan, Mannedorf, Switzerland) to quantify the amount of biofilm ($n = 5$).

Exopolysaccharides (EPS) quantification assay: Following treatment in the absence and presence of 1-mg/mL of nano-PLGA:RF/VE-TPGS_{0.50}, and nano-PLGA:RF/VE-TPGS_{0.50}:k21 (all k21 concentrations) for 24 h, bacterial cultures were washed with 0.9% NaCl, supplemented with equal volume of 5% phenol and 5 vol of H₂SO₄. Plates were stored in dark for 1 h and centrifuged at 16,770 g for 10 min s. Absorbance was recorded at OD₄₉₀ ($n = 5$).

Biofilm detachment assay: For assessing biofilm detachment, protocol was adapted with modifications from elsewhere [30]. Bacterial cultures treated with 1-mg/mL of nano-PLGA:RF/VE-TPGS_{0.50}, nano-PLGA:RF/VE-TPGS_{0.50}:1%k21, and nano-PLGA:RF/VE-TPGS_{0.50}:2%k21 and nano-PLGA:RF/VE-TPGS_{0.50}:3%k21 were incubated in 96-well plate for 24 h without agitation. About 3 µL of 10% SDS was added to each well and incubated for 30min. Absorbance of suspended cells was measured at OD₅₉₅ ($n = 5$).

2.8. Nanoparticles delivery to demineralized dentine-substrates

Clinically extracted non-carious non-restored human molars ($n = 48$) from patients aged 21–35 years were used as *ex-vivo* models. Ethical approval was obtained in accordance with guidelines from the Institution Review Board for the research use of extracted human teeth. Demineralized dentine disc-shaped specimens were prepared as mentioned earlier [31,32]. Briefly, collected teeth were stored in 0.5% Chloramine-T solution at 4 °C for 2 weeks and used within two months from point of extraction. The extracted teeth were sectioned with low speed diamond blade to obtain ~ 1 -mm dentin discs, polished using SiC papers of 600 grit-size (Carbimet; Buehler, Lake-Bluff, IL, USA), ultrasonically cleaned, etched using 35% phosphoric acid for 15s, rinsed and gently dried with compressed air.

An *ex-vivo* experimental set-up was built to simulate intra-pulpal pressure (-560 , and ± 0 mmHg in the case of negative pressure, with the chamber and pulpal cavity were filled with distilled water for positive pressure status. to facilitate nanoparticle delivery to demineralized dentin-substrates as reported previously [28]. nano-PLGA:RF/VE-TPGS_{0.50} and nano-PLGA:RF/VE-TPGS_{0.50}:k21 specimens (at 1-mg/mL) were suspended in distilled water at 13.7% (w/v), corresponding to k21 total content (w/v) of 4.51% (nano-PLGA:RF/VE-TPGS_{0.50}:k21) based on the k21 entrapment into the nanoparticles. About 15 µL of the nanoparticle suspension was added in dropwise manner to dentine specimens, micro-brush rubbed for 5s, gently air blown and dried by a wet cotton-pellet. The blue light source used was placed 10 mm from dentine surface with a spot size of 7 mm, such that whole dentine specimen was fully irradiated with a single blue light irradiation spot. SEM/TEM investigations were done to study nanoparticles. Samples were dried for 48 h at room temperature, sputter-coated and processed for SEM examination ($n = 5$). For TEM viewing, samples were prepared and processed as described previously [28].

2.9. Resin-dentin bonding and anti-biofilm investigation

Following nanoparticles delivery, dentine specimens were bonded using a two-step etch-and-rinse according to manufacturer's instructions. Bonded specimens were randomly grouped for two types of experiments: (i) antibiofilm studies and (ii) investigation of resin-dentine interfacial bonding and micro-tensile bond strength testing. After bonding procedure, *S. mutans* biofilms were cultivated on surface of resin bonded dentin-substrates. Specimens were placed in 24-well plates containing 1.5 mL of sterile BHI media and 250 µL of the

bacterial suspension, incubated for 48 h at 37 °C in a 5% CO₂ to facilitate biofilm formation ($n = 7$).

Following incubation, specimens were washed with sterile PBS, fixed with 2% glutaraldehyde for 1-week and sequentially dehydrated in ascending ethanol concentrations of 70%, 80%, 85%, 90%, 95% (v/v) (for 24 h each) and 100% (for 48 h). Specimens were desiccated by critical point drying (Balzers 030, Shimadzu, Kyoto, Japan), mounted on metal stubs using double coated carbon tapes, sputter coated and viewed by SEM ($n = 5$ per group).

For live/dead assay, *S. mutans* biofilms harvested on bonded dentine substrates for 48 h were stained with Film Tracer™ LIVE/DEAD Biofilm Viability kit (Life Technologies-Invitrogen, Grand Island, NY, USA). The dyes (SYTO9 and propidium iodide) (ratio of 1:1 wt/v) were utilized according to manufacturer's instructions. Dentine specimens were stained for 20 min in dark at room temperature and treated with distilled water to remove the excess stain. Some specimens ($n = 3$) were stained using 0.1 wt % aqueous solution of sodium fluorescein (46,960 Bio-reagent, Millipore Sigma) for non-destructive identification of k21 within the resin–dentine interface. Samples were later imaged using confocal laser scanning microscope (OLYMPUS FLUOVIEW FV1000; Olympus, Tokyo, Japan) ($n = 5$ per group).

For confocal analysis, a transcendental model was acquired [33]. Briefly, dentine discs for the groups ($n = 7$) was performed by evaluation of the dentine permeability of each dentine disc. After smear layer removal (0.5 M EDTA (pH 7.4) for 60 s), the discs were washed and placed in diffusion chamber connected for 5min in 200 cm column of water. The movement of a micro-bubble introduced through a metal cannula was recorded for 1min and hydraulic conductance (L_p) of dentine was calculated using the mathematical equation:

$L_p = J_v / At(P)$ where

L_p = hydraulic conductance in $\mu\text{L cm}^{-2}, \text{min}^{-1}, \text{H}_2\text{O}^{-1}$

J_v = fluid flow in $\mu\text{L min}$

A = surface area of the dentine in cm^2

t = time

P = hydrostatic pressure applied in $\text{cm H}_2\text{O}$.

Then, an area of 0.28 cm^2 was standardized using a metallic ring on dentine disc, and a fresh smear layer was created using 600-grit silicon carbide paper. Bacteria were cultured as mentioned previously and seeded on pulpal side of dentine discs (0.28 cm^2) in 24-well plates ($n = 5$). Discs were transferred back to same wells with occlusal side up to receive nanoparticle treatments. Nanoparticle formulation was applied onto occlusal side of dentine discs using a sterile micro brush for 20 s, followed by blot-drying. All procedures were performed in a vertical laminar flow hood. After treatment, dentine discs were returned to CO₂ incubator for an additional 24 h.

2.10. Characterization of resin-dentine interface and μTBS testing

Nanoparticle-infiltrated resin-bonded dentine specimens were subsequently restored with a resin-based restorative composite as reported previously. Briefly, a crown of ~4 mm was built in equal increments and cured for 20s using a light emitting diode curing light (COXO). Restored teeth were stored in distilled water for 24 h at 37 °C to complete the process of polymerization.

Restored dentine specimens were sectioned at right angles to resin-dentine adhesive interface to obtain ~1 mm resin-dentin slabs and stored in distilled water for 48 h at 37 °C. Following storage, dentin slabs were polished using SiC papers, cleaned ultrasonically, etched with 35% phosphoric acid gel for 15s, rinsed for 15s and dried with compressed air. Specimens were then exposed to 5.25% sodium hypochlorite solution for 20 min and rinsed with running water for 5 min. Later, slabs were fixed with osmium tetroxide solution, washed with PBS solution for 10-mins (twice) followed by distilled water for 1 min, dehydrated in increasing concentrations of ethanol and finally desiccated using critical

point dryer (as mentioned earlier). Sputter-coated resin-dentin slabs were viewed at an accelerating voltage of 10 kV, and images of resin-dentine interface at selected representative areas were captured at different magnifications ($n = 5$).

Remaining restored teeth specimens were sectioned in x-y directions parallel to adhesive interface and resin-dentin beams of ~1-mm \times 0.9-mm were obtained. Specimens were stored in distilled water for 1 month at 37 °C and replenished weekly ($n = 21$ per group). Resin-dentine beams were fixed on custom-prepared metal jigs with cyanoacrylate adhesive (Zapit, Dental Ventures of America, USA) and mounted on a universal testing equipment (Instron, 5848 Microtester, USA). Dimension and surface area of each beam was measured using a digital caliper (CD-6, Mitutoyo Corporation, Japan) and stressed to failure with a 50 N load cell at a cross-head of 1-mm/min. μTBS values (MPa) were calculated by dividing maximum load (N) by respective surface area (mm^2).

2.11. Molecular simulation

A small-molecule drug discovery suite (Schrödinger, LLC, NY, USA; Version 2018–2) was used to obtain insights on binding of the quaternary ammonium silane to the active sites on MMP-2 and MMP-9 enzymes. The 3D structures were downloaded from Research Collaboratory for Structural Bioinformatics Protein Data Bank (PDB; <http://www.pdb.org>).

2.12. Raman spectroscopy

Raman spectra (Senterra Raman microscope (Bruker Optics, Ettlingen, Germany; 532 nm and 785 nm lasers Jobin Yvon) were collected between a wave number region of 400 cm^{-1} – 3200 cm^{-1} using e OPUS 6.5 spectral acquisition, the 785 nm laser. The backgrounds were collected after every 1000s with higher resolution spectra over a narrow spectral region ($\times 100/\text{NA}$ 0.9 objective) with the single band reproducibility within 0.5 cm^{-1} . Each spectrum was a composition of 30 spectra for 10 s scanning using incident laser power of <500 μW .

2.13. Collagenase-mediated degradation resistance

Assay kit (BioVision, Exton, PA, USA) was used to measure hydroxyproline (HYP) content in supernatant at 48 h in collagenase. Dentine slabs (4.5 mm \times 3.5 mm \times 0.5 mm) randomly distributed between four groups ($n = 5$), demineralized in phosphoric acid, and treated as described above. Specimens were exposed to 100 gml^{-1} of bacterial collagenase type 1 in tricine buffer for 24 h. HCl (12 M) were used to hydrolyze 100 μL aliquots at 120 °C for 3 h. From the 100 μL aliquots, 10- μL quantities were transferred to a 96-well plate for evaporation under vacuum and Chloramine-T buffer reagent (100 μL) added, and solutions incubated at 27 °C for 5 min 100 μL of DMAB reagent was added later, incubated for 90 min at 60 °C and absorbance measured using a spectrophotometer (Ultramark; Bio-Rad, Hercules, CA, USA) at 560 nm.

2.14. Statistical analysis

Results were shown as mean \pm standard deviation values and analyzed by ANOVA followed by Tukey-Kramer post hoc test was used to evaluate our reported values using SPSS Statistics 15.0. P -values <0.05 were considered statistically significant.

3. Results

3.1. Nanoparticle characteristics

Physicochemical properties of PLGA:RF/VE-TPGS_{0,50}, nano-PLGA:RF/VE-TPGS_{0,50}:k21 (different concentrations), and nano-

PLGA:RF/VE-TPGS_{0.50}:Blank are shown in Table 1. The nanoparticle preparation technique resulted in nano-PLGA:RF/VE-TPGS_{0.50} having a diameter of $\sim 122.44 \pm 24.03$ nm. Incorporation of -k21 to the system favoured an increase in the colloidal size to $\sim 135.76 \pm 17.6$ nm, $\sim 133.9 \pm 15.53$ nm and $\sim 142.3 \pm 28.62$ nm for nano-PLGA:RF/VE-TPGS_{0.50}:1%k21, nano-PLGA:RF/VE-TPGS_{0.50}:2%k21 and nano-PLGA:RF/VE-TPGS_{0.50}:3%k21 respectively. Accordingly, the negative zeta potential of nano-PLGA/Blank at -20.1 ± 0.11^a mV reached a significant low value. In addition, a perturbing the surface charge of the colloidal system with increasing addition of k21 was seen. On the other hand, the polydispersity index evidenced a slight increase when k21 was entrapped in the polymer matrix, indicating nanoparticles within narrow size range and uniform distribution (Table 1). SEM micrographs revealed intact, uniform sized, spherical nanoparticles with a positive trend upon k21 addition (Fig. 1a–c). Dimensional homogeneity and smooth texture of nanoparticles was confirmed as shown in Fig. 1a–c. No significant change in surface morphology was observed upon k21 and nano-RF/VE-TPGS_{0.50} incorporations.

3.2. Drug loading, encapsulation and release profile

Fig. 2 shows percentage release of RF from all samples at different time intervals after 28 days. The riboflavin release profiles from k21 embedded nanoparticles consist of a burst release (steeper in nano-RF/VE-TPGS_{0.50} specimens) followed by a gradual release phase over the 3 days. However, the burst was not seen in 2 and 3%k21 specimens at the initial phase within 3 days. Upon inclusion of the drug, % encapsulation of PLGA:RF/VE-TPGS_{0.50}:1%k21 was $35.35 \pm 20.53\%$ as shown in Table 1. With increasing addition, the values noticeably escalated to $43.93 \pm 19.42\%$ and $52.36 \pm 23.73\%$, for PLGA:RF/VE-TPGS_{0.50}:2%k21 and PLGA:RF/VE-TPGS_{0.50}:3%k21, respectively. The *in vitro* k21 release pattern from nanoparticles up to ~ 28 days is shown in Fig. 2b. Nano-PLGA:RF/VE-TPGS_{0.50}:k21 at percentages of 1, 2 and 3% show an initial k21-burst of $15.83 \pm 6.35\%$, $22.13 \pm 4.25\%$ and $45.95 \pm 9.54\%$ for the first 6 h followed by a slow sustained release of $46.11 \pm 4.62\%$, $63.46 \pm 7.36\%$ and $77.82 \pm 6.74\%$ respectively.

3.3. In vitro cytotoxicity

Initial nanoparticle toxicity tested by MTT assay indicated nano-PLGA:RF/VE-TPGS_{0.50}:k21 1%, 2% and 3% at concentrations of 0.5 and 1-mg/mL showed $>60\%$ viability as compared to 2-mg/mL. Nano-PLGA:RF/VE-TPGS_{0.50}:3%k21 did not disturb the cell viability at all concentrations as shown in Fig. 2c. Significant differences were noted between experimental and control groups. Considering the importance of toxicity of these nanoparticles, only 1-mg/mL of nano-PLGA:RF/VE-TPGS_{0.50} blank, nano-PLGA:RF/VE-TPGS_{0.50}:1%k21 and nano-PLGA:RF/VE-TPGS_{0.50}:3%k21 were used for further experiments, except for bond strength.

Table 1

Average size (nm), Zeta Potential (ζ) (mV), Polydispersity Index (PDI) and Drug Encapsulation (%) of nano-PLGA/Blank, nano-PLGA:RF/VE-TPGS_{0.50}:1%k21, nano-PLGA:RF/VE-TPGS_{0.50}:2%k21 and nano-PLGA:RF/VE-TPGS_{0.50}:3%k21 respectively. μ TBS (in MPa) of control specimens (without nanoparticle exposure) and nano-PLGA:RF/VE-TPGS_{0.50}:Blank and nano-PLGA:RF/VE-TPGS_{0.50}:2%k21 treated specimens following 12-month storage in distilled water at 37 °C. *Groups with different alphabets are considered statistically significant (Tukey's test; $p \leq 0.05$).

Groups	Average Size (nm)	Zeta Potential (ζ) (mV)	Drug Encapsulation k21 (%)	μ TBS Mpa (immediate)	μ TBS Mpa (12-months)
Control no nanoparticle	–	–	–	38.6 ± 7.6^a	$22.5 \pm 4.9\alpha$
Plga blank	138.6 ± 19.7^a	-20.1 ± 0.11^a	–	36.3 ± 4.4^a	$23.7 \pm 8.1 \alpha$
Nano- PLGA:RF/VE-TPGS _{0.50}	122.44 ± 24.03^b	18.95 ± 0.11^a	–	40.12 ± 5.1^a	$29.67 \pm 6.8 \beta$
Nano- PLGA:RF/VE-TPGS _{0.50} :1%k21	135.76 ± 17.6^a	24.6 ± 3.57^b	35.35 ± 20.53^a	–	–
Nano- PLGA:RF/VE-TPGS _{0.50} :2%k21	133.9 ± 15.53^a	35.85 ± 8.45^c	43.93 ± 19.42^{ab}	–	–
Nano- PLGA:RF/VE-TPGS _{0.50} :3%k21	142.3 ± 28.62^c	43.97 ± 12.18^c	52.36 ± 23.73^b	37.7 ± 7.1^a	$33.67 \pm 6.8 \lambda$

*Groups with different superscript letters indicate statistical significance ($P \leq 0.05$) within each column. Values were analyzed by ANOVA followed by Tukey-Kramer post hoc test.

3.4. Nanoparticle antibacterial/antibiofilm properties

Agar disc diffusion assay: Treatment of planktonic bacterial cultures with PLGA:RF/VE-TPGS_{0.50}:k21 confirmed the antibacterial effect of nanoparticles as indicated in Table 2. With an increase in k21 loading, an increased antibacterial zone was obtained. As a result, 3%k21 exhibited the most antibacterial effect as compared to 1% and 2%k21 treated specimens.

Biofilm inhibition assay: The effect of nanoparticles on biofilm formation assessed by crystal violet assay (Table 2) indicated that at 1-mg/mL, nano-PLGA:RF/VE-TPGS_{0.50}:1%k21 and PLGA:RF/VE-TPGS_{0.50}:3%k21 dislodged $>48\%$ and $>57\%$ from preformed *S. mutans* biofilm, in comparison to nano-PLGA:Blank ($<12\%$) and nano-PLGA:RF/VE-TPGS_{0.50}:2%k21 ($>52\%$).

Elimination of EPS: Nano-PLGA/GO at ratios of 1% ($\sim 38\%$) and 3% ($\sim 50\%$) significantly minimized EPS production in *S. mutans* after nanoparticle exposure at 1-mg/mL (Table 2). EPS reduction by nano-PLGA:RF/VE-TPGS_{0.50}:Blank was significantly lower ($\sim 24\%$) as compared to nano-PLGA:RF/VE-TPGS_{0.50}:k21 specimens (nano-PLGA:RF/VE-TPGS_{0.50}:2%k21 specimens/ $\sim 43\%$).

Biofilm detachment assay: In all the groups (nano-PLGA:Blank, nano-PLGA:RF/VE-TPGS_{0.50}:k21mspecimens) biofilms were detached by SDS as shown in Table 2. However, the overall detachment efficiency for biofilms exposed to 3% k21 nanoparticles ($\sim 83\%$) was higher, indicating that samples were loosely attached to the surface than that for biofilms without k21 treatment ($\sim 26\%$). Specifically, nano-PLGA:RF/VE-TPGS_{0.50}:k21 treated samples exhibited higher detachment as compared to nano-PLGA:Blank. From the anti-planktonic bacteria and the antibiofilm studies, it is evident that 1-mg/mL of nano-PLGA:RF/VE-TPGS_{0.50}:2%k21 exhibited maximum antibacterial property as compared to the nano-PLGA:Blank and Nano-PLGA:RF/VE-TPGS_{0.50}:1%k21. Therefore, further investigations involving dentine experiments employed only 1 mg/mL of nano-PLGA:RF/VE-TPGS_{0.50}:3%k21 (for reference purpose).

3.5. Nanoparticles delivery to demineralized dentin-substrates

Representative SEM micrographs shown in Fig. 3a and b indicate successful deep infiltrative capacity of nanoparticles inside the dentinal tubules. Nanoparticles were seen confined and clustered inside the tubules. However, the morphological integrity of nanoparticles remained unchanged upon delivery. Both nano-PLGA:RF/VE-TPGS_{0.50}:1%k21 and nano-PLGA:RF/VE-TPGS_{0.50}:3%k21 showed similar infiltration results displaying nanoparticles held within the vicinity of the dentinal tubules of the collagen network of demineralized dentin-substrates (Fig. 3b). CLSM merged image after application of 3% k21 and adhesive is exhibited in Fig. 3C, with sodium fluorescein staining of k21. The adhesive and dentine exhibited slight background auto fluorescence. QAS/k21 was displaced by the adhesive down the dentinal tubules (arrows). The top

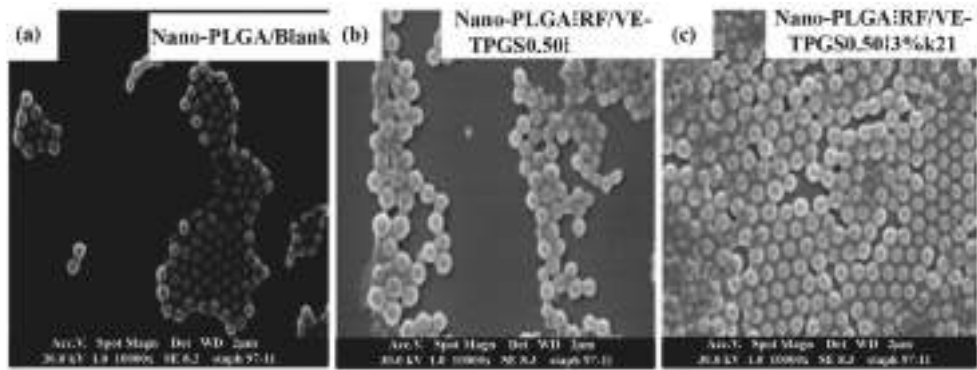


Fig. 1. Selected high magnification SEM (a–c) micrographs confirming the uniform-sized, smooth textured spherical nanoparticles of the nano-PLGA/Blank and nano-PLGA-RF/VE-TPGS_{0.50i} and nano-PLGA-RF/VE-TPGS_{0.50i}:3%k21 nanoparticles respectively.

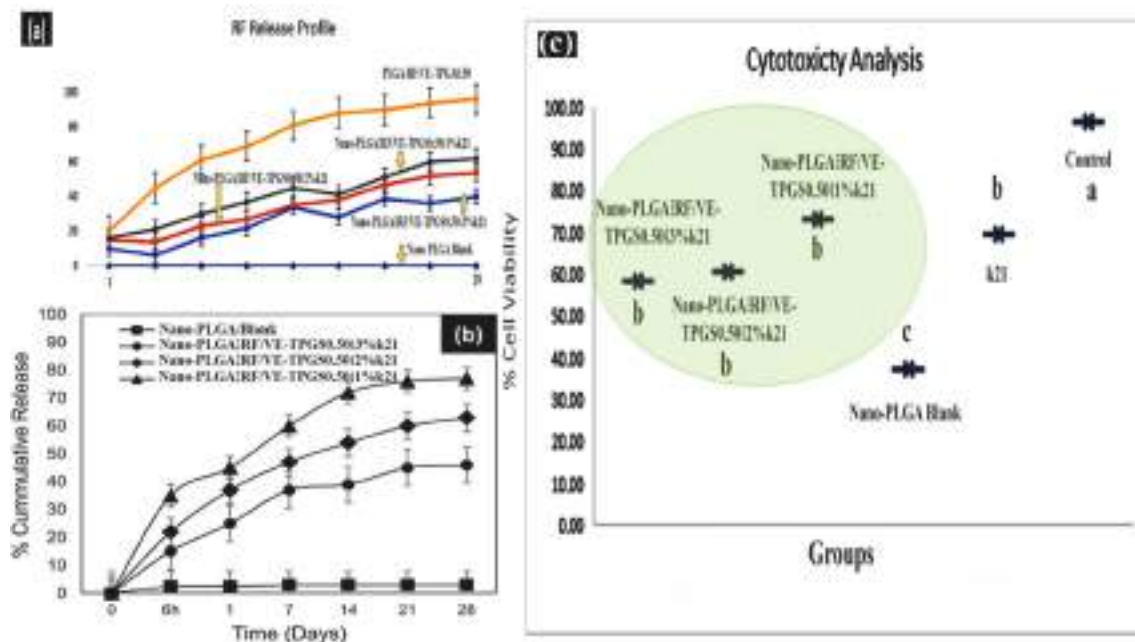


Fig. 2. (a) Representative riboflavin release specific to, nano-PLGA/Blank and nano-PLGA-RF/VE-TPGS_{0.50i}:k21 at different concentrations. (b) Percentage (%) k21 cumulative *in vitro* release from formulations of nano-PLGA/k21 nanoparticles at the PLGA/k21 ratios of 1, 2 and 3% in PBS (pH 7.4) at 37 °C up to 28 days. Nano-PLGA/Blank was considered as control. *Statistical analysis of *in vitro* k21 release was done with one-way ANOVA, followed by Tukey–Kramer post hoc test ($P \leq 0.05$). (c) Box whisker showing percentage (%) cell viability of hMSCs following treatment with 1, 2 and 3% (k21) of nano-PLGA-RF/VE-TPGS_{0.50i}:k21, nano-PLGA/Blank and k21 respectively. *Box-whisker displaying different alphabets are statistically significant ($P \leq 0.05$). **Statistical analysis was performed with one-way ANOVA followed by Tukey–Kramer post-hoc test.

50 mm of dentine did not contain stained tags. This area corresponds to resin tags formed by the dentine adhesive. The specimens show long formed resin tags showing the presence of nanoparticles trapped deep and closely associated with their morphological structure.

3.6. Resin-dentin interfacial morphology and μ TBS testing

SEM investigation of resin-dentine adhesive interface (Fig. 4d and e) showed formation of intact homogenous hybrid-layer with well-developed resin-tags upon application of the etch-and-rinse (E&R) dentine bonding agent to demineralized dentin substrates modified with nano-PLGA:RF/VE-TPGS_{0.50i}:3%k21. Upon bonding resins infiltration and polymerization, nanoparticles inside the tubules are closely associated and overlapped with the resin tags formed by the infiltrating bonding resin monomers (Fig. 4f). Moreover, nanoparticles were delivered to considerable depths inside the dentinal tubules and were

found to be associated with and below the resin tags, attached and embedded in dentin collagen matrix. μ TBS analysis of resin-dentine bonded specimens infiltrated with 1-mg/mL of nano-PLGA:RF/VE-TPGS_{0.50i} and Nano-PLGA:RF/VE-TPGS_{0.50i}:3%k21 specimens are shown in Table 1. After 12-months storage in distilled water, dentine specimens treated with nano-PLGA:RF/VE-TPGS_{0.50i}:3%k21 showed significant improvement in μ TBS as compared to the control group. There were significant differences between nano-PLGA:RF/VE-TPGS_{0.50i}:3%k21 groups and nano-PLGA:RF/VE-TPGS_{0.50i} groups after 12 months and showed the highest bond strength values, indicating that the short-term bond strength values were either unaffected or improved with use of nanoparticles application and delivery to demineralized dentine substrates till 3%k21 concentrations used.

Table 2

Inhibition zone diameters obtained from agar-disc diffusion method with *S. mutans* after treatment with 1 mg/mL of nano-PLGA:Blank, PLGA:RF/VE-TPGS_{0.50}:1%k21, 2% and PLGA:RF/VE-TPGS_{0.50}:3%k21, respectively.

Bacterial strains used	Diameters of the inhibition zone (cm) obtained after treatment with						
	Nano-PLGA:Blank	PLGA:RF/VE-TPGS _{0.50} :1%k21		PLGA:RF/VE-TPGS _{0.50} :2%k21		PLGA:RF/VE-TPGS _{0.50} :3%k21	
			Nanoparticle	Pure k21 +ve ctrl	Nanoparticle	Pure k21 +ve ctrl	Nanoparticle
<i>S. mutans</i> %inhibition	0.58 ± 0.05 ^a	1.42 ± 0.21 ^b	1.68 ± 0.04 ^b	2.22 ± 0.08 ^b	2.64 ± 0.2 ^b	3.52 ± 0.25 ^c	2.71 ± 0.12 ^c
Biofilm	<12%	>48%		>52%		>57%	
EPS	~24%	~38%		~43%		~50%	
Biofilm Detachment <i>S.mutans</i>	~26%	69%		76%		83%	

*Groups with different superscript letters indicate statistical significance (p ≤ 0.05) within each row. Values were analyzed by ANOVA followed by Tukey-Kramer post hoc test.

3.7. Biofilm inhibition on resin-infiltrated dentin-substrates

Antibiofilm effect of nanoparticles modified demineralized dentine-substrates after bonding resin infiltration was evaluated in term of biofilm eradication and cells viability using SEM and CLSM. Representative SEM findings (Fig. 4a–c) validated CLSM results and confirmed the biofilm disruption potency of nanoparticles with utmost biofilm impairment, detachment and eradication by nano-PLGA:RF/VE-TPGS_{0.50}:3%k21. Representative CLSM images revealed the presence of large number of viable cells on the surface of control (Fig. 4d) and the nano-PLGA:RF/VE-TPGS_{0.50}:1 (1-mg/mL) containing (Fig. 4e) resin-infiltrated dentin specimens. Dentine specimens modified with 1-mg/mL of the nano-PLGA:RF/VE-TPGS_{0.50}:3%k21 (Fig. 4f and g) showed obvious biofilm disintegration, non-viable cells and demonstrated the greatest eradicating effect.

3.8. Molecular simulation (MMP profilometry) and Raman spectroscopy

Fig. 5B indicates a schematic detailed ligand atom interaction with the protein residues of Sortase-A with k21 molecule. Interactions that occur more than 5.0% of simulation time in the selected trajectory (0.00 through 100.00 nsec), are shown. It is possible to have interactions with >100% as some residues may have multiple interactions of a single type with same ligand atom. The side chain four H-bond donors that can all

hydrogen-bond to a single H-bond acceptor. A larger Site Score (0.995352) and DScore (1.019596) were selected as binding pockets for molecular docking studies with MMP-2 (PDB ID: 3AYU). 3D binding pose of key amino acids involved in binding of quaternary ammonium silane to MMP-2 and -9 are shown in Fig. 5 C–F. XP GScores of quaternary ammonium silane were –2.383 and –4.383 for MMP-2 and -9 respectively.

Chemical compositions of biofilms caused by different treatments were characterized using Raman spectroscopy. The most prominent peak 1450 cm⁻¹ was used to normalize the specimens. The peak was assigned to deformation of C–H functional groups in carbohydrates and showed lower intensities in nano-PLGA:RF/VE-TPGS_{0.50}:k21 groups (Fig. 5G). Apart from variations around 1450 cm⁻¹, peak variations were also observed at 785 cm⁻¹ as intensities were lowered (Fig. 5H). Peak intensity of 785 cm⁻¹ nano-PLGA:RF/VE-TPGS_{0.50}:3%k21 and nano-PLGA:RF/VE-TPGS_{0.50}:1%k21 treated groups was lower than that in the untreated control and nano-PLGA:RF/VE-TPGS_{0.50}: treated groups. These peaks were assigned to ring breathing mode of DNA/RNA such as adenine, cytosine, guanine, thymine and uracil. The lower intensities indicated the damage or disruption of nucleic acids in bacterial cells.

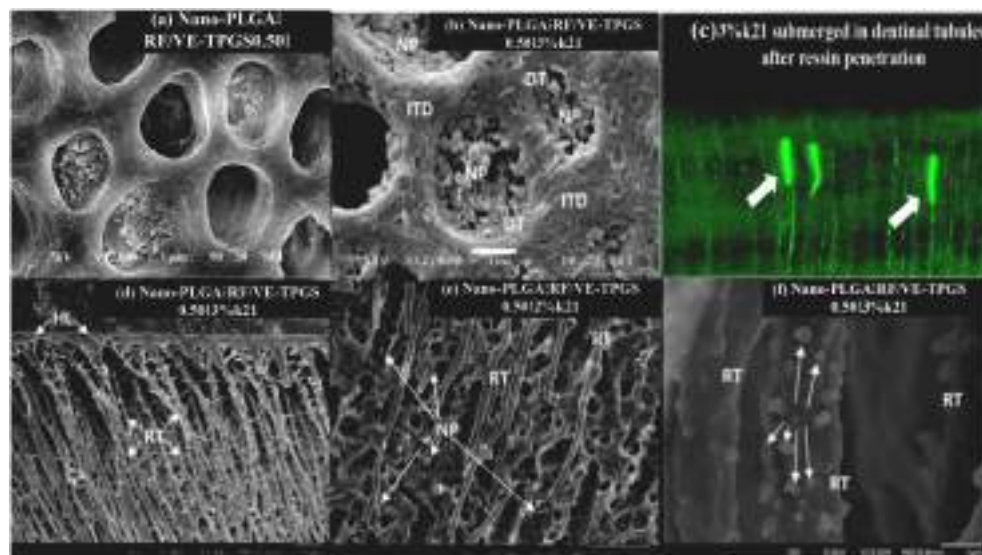


Fig. 3. Representative (a–b) SEM, (c) confocal image showing successful infiltration of (a) nano-PLGA:RF/VE-TPGS_{0.50}:Blank and (c) nano-PLGA:RF/VE-TPGS_{0.50}:3%k21 inside demineralized dentinal tubules. (c) CLSM merged image after application of 3% k21 and adhesive, with sodium fluorescein staining of the QAS. The adhesive and dentine exhibited slight background auto fluorescence. The QAS was displaced by the adhesive down the dentinal tubules (arrows). The top 50 mm of dentine did not contain stained tags. This area corresponds to resin tags formed by the dentine adhesive. (d–e) intact hybrid-layer with long formed resin tags (f) showing the presence of nanoparticles trapped deep and closely associated with their morphological structure.

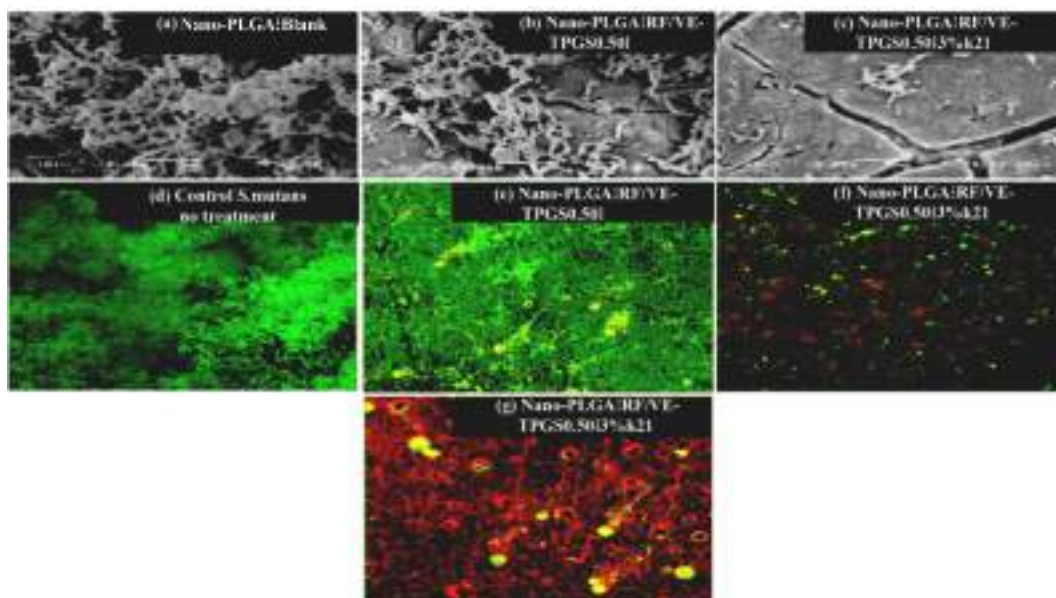


Fig. 4. Representative SEM/CLSM images showing biofilm inhibition on restored dentine specimens without nanoparticle exposure (a); after exposure to nano-PLGA:Blank; (b) Nano-PLGA:RF/VE-TPGS_{0.50}; (c) treatment with nano-PLGA:RF/VE-TPGS_{0.50}:3%k21; (d–e) CLSM image of control and after exposure to nano-PLGA:RF/VE-TPGS_{0.50} specimens and (f–h) nano-PLGA:RF/VE-TPGS_{0.50}:3%k21 after 48 h showing biofilm inhibitory potential of nanoparticles.

3.9. Collagenase-mediated degradation resistance

HYP liberation was recorded reflecting higher collagenase degradation resistance with nano-PLGA:RF/VE-TPGS_{0.50} (2.9 ± 5.6) specimens including RF/VE-TPGS formulations (Fig. 6). In groups nano-PLGA:RF/

VE-TPGS_{0.50}:3%k21 (1.1 ± 3.1), and 3% pure k21 solutions (0.8 ± 0.9), there was significant decreased HYP liberation compared with control (6.34 ± 3.4) specimens after 24 h.

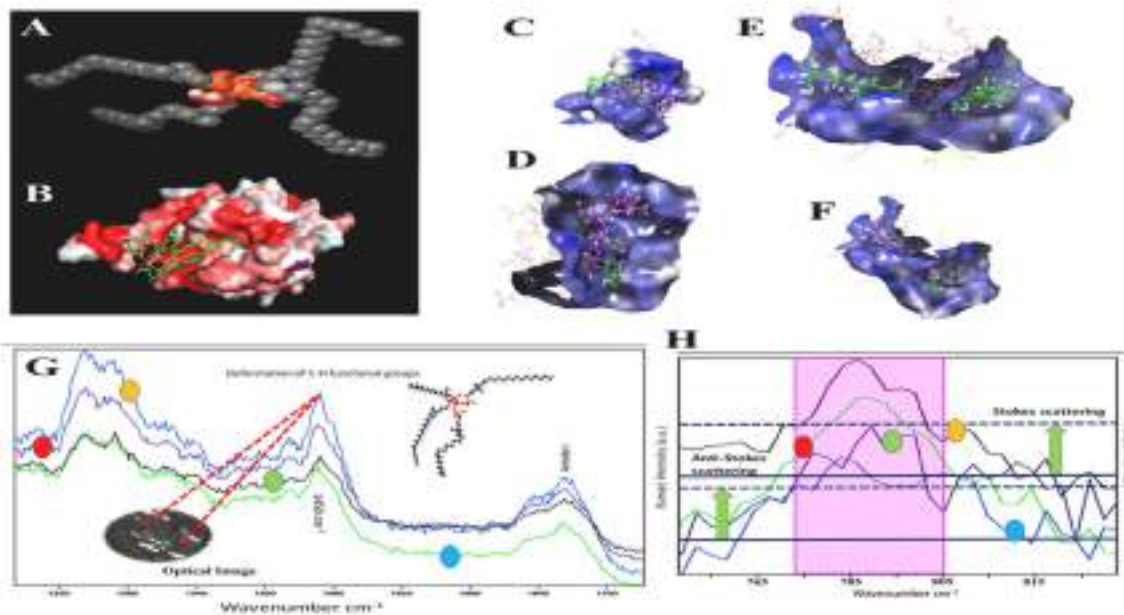


Fig. 5. (A) Molecular docking simulation of k21 2% molecule showing sol-gel reaction product between 3-(triethoxysilyl)-propyldimethyloctadecyl ammonium chloride and tetraethoxysilane; codenamed K21; C92H204Cl4N4O12Si5; CAS number 1566577-36-3), reacting 3-(triethoxysilyl)-propyldimethyloctadecyl ammonium chloride with tetraethoxysilane as the anchoring unit; (B) Results of molecular docking simulation of k21 2% on crystal structure of SrtA indicating a complex indicating a predicated interaction mode of k21 catalytic center of SrtA; optimized geometries of k21 2% with (C) collagen, (D) MMP-9, (E–F) MMP-2 complexes; (G–H) Raman spectra representing biofilm changes. (G) Control (orange circle); nano-PLGA:RF/VE-TPGS_{0.50} (red circle); nano-PLGA:RF/VE-TPGS_{0.50}:1%k21 (green circle); nano-PLGA:RF/VE-TPGS_{0.50}:3%k21 (blue circle) (H) The peak intensity of 785 cm⁻¹ nano-PLGA:RF/VE-TPGS_{0.50}:3%k21 (blue circle) and nano-PLGA:RF/VE-TPGS_{0.50}:1%k21 (green circle) treated groups was lower than that in the untreated control (orange circle) and nano-PLGA:RF/VE-TPGS_{0.50} (red circle) treated groups. (For interpretation of the references to color in this figure legend, the reader is referred to the Web version of this article.)

4. Discussion

Development and delivery of drug-loaded nanocarriers targeting treatment of dental diseases caused by bacterial colonization and bio-film formation are attracting recent research attention [34]. Nanotechnology facilitates efficient use of compounds which otherwise may pose a risk due to low bio-absorption or when used in high concentrations over short intervals of time [35]. In our earlier works, we introduced a novel drug delivery mechanism to demineralized dentin-substrates and resin-dentin adhesive interface using biodegradable drug loaded/encapsulated nanocarriers through dentinal tubules for controlled release of drugs [20–36]. Nano-PLGA:RF/VE-TPGS_{0.50}:k21 were formulated through an efficient and reproducible manner. Combined effect of biodegradable lipophilic groups and biocompatible RF/VE-TPGS_{0.50}:k21 groups has entrapped drug and simultaneously improved its encapsulation. Different drug-to-polymer ratios were explored to attain acceptable nanoparticle size with maximum drug encapsulation (Table 1). It could be observed that particle size measured from SEM was smaller than DLS values due to dry preparatory conditions of SEM [37]. Spherical nanoparticles with particle size less than 200 nm, smooth texture, high k21 encapsulation were considered conducive for infiltration studies (Fig. 3a–c and Table 1).

For nano-PLGA:RF/VE-TPGS_{0.50}:k21 to effectively release k21 without undergoing aggregation, PVA was chosen as surfactant owing to its amphiphilic property and water solubility for maintaining dimensional stability of nanoparticles [38]. Based on the hydrophobic nature of k21 [10], it can be adsorbed or dispersed into polymeric PLGA matrix. It is when the bonds disseminate, and drug gets released [20]. With initial k21 burst of ~6 h followed by sustained k21 release disseminated from the core of nano-PLGA:RF/VE-TPGS_{0.50}:k21 (Fig. 2b), it is expected that the drug gets released beyond the speculated time frame of 28 days to complete the process of release-kinetics. Zeta-potential is an important deciding factor of nanoparticle stability. Upon k21 loading, the obtained values indicate combined electrostatic and steric stabilization (Table 1) where repulsion between nanoparticles prevents aggregation and facilitates easy redispersion [39,40]. This can also be due to k21 surfactant effectively lining the interface. These functional nanoparticles contain a positive charge on their surface between the primary amine and quaternary ammonium moieties and a biodegradable hydrophobic portion due to PLGA. This results in a more positive zeta potential as compared to controls. However, there may be few limiting factors like practical limits of available techniques and

instruments. If centrifugation is the only method, the speeds of centrifuge create a bottleneck for the lowest particle size that can be recovered as sediment.

While the smooth shape of PLGA:RF/VE-TPGS_{0.50}:k21 may reduce tissue irritation in comparison to crystalline and irregular particles, it should always be considered to have biocompatible antimicrobials because of the potential of reaching the dental pulp when these materials are being applied to deep, smear layer-depleted dentine. The present study compared ex-vivo biocompatibility of PLGA:RF/VE-TPGS_{0.50}:k21 after these nanoparticles were in contact with human mesenchymal stem cells for 24 h. 0.4 mm thick dentine discs were used as a standard model for evaluation of transdentinal cytotoxicity simulating optimum clinical situation [41]. Moreover, decline in cell viability at 48 h could also be ascribed to increasing nanoparticle concentrations and drug encapsulation as observed with PLGA:RF/VE-TPGS_{0.50}:3%k21 (Fig. 2c). However, in a clinical setting, demineralization depth limits deep penetration of nanoparticles and prevents it from contacting pulp whereas dentinal fluid might alleviate cytotoxicity to some extent [33]. Moreover, the use of RF/VE-TPGS within the formulation has provided major impetus without any cytotoxic implications. Our previous studies have indicated that use of this crosslinking equation with adhesives to macrophage polarization profile was a predominantly M2 anti-inflammatory phenotype, facilitating tissue repair and regeneration [42]. These findings suggested that regulating ratio of M1 to M2 provided a novel therapeutic strategy. Further studies are required to elucidate the mechanisms responsible for the more favourable biocompatibility of PLGA:RF/VE-TPGS_{0.50}:k21 nanoparticles.

Antibacterial activity of k21 molecule have been validated earlier [8]. Because of the presence of long hydrocarbon chains, k21 increases hydrophobicity of demineralized dentine by changing its surface energy [43]. In addition to this, water from dentinal tubules is consumed during hydrolysis of k21 silanol groups reducing residual water and increasing wetting of adhesive improving adhesive polymerization [44,45]. These factors may have contributed to good bond strength associated with use of experimental PLGA:RF/VE-TPGS_{0.50}:k21 nanoparticles. Streptococcus mutans are cariogenic oral pathogens associated with secondary caries [46]. These residual bacteria can persist after cavity preparation and may reside in dentinal tubules. PLGA:RF/VE-TPGS_{0.50}:k21 nanoparticles readily flowed inside dentinal tubules with adhesive impregnation (Fig. 4f) to kill any intratubular bacteria. It can be inferred that encapsulation of k21 into PLGA has only improved its antibacterial activity by rupturing the cells. Here, antimicrobial profile of

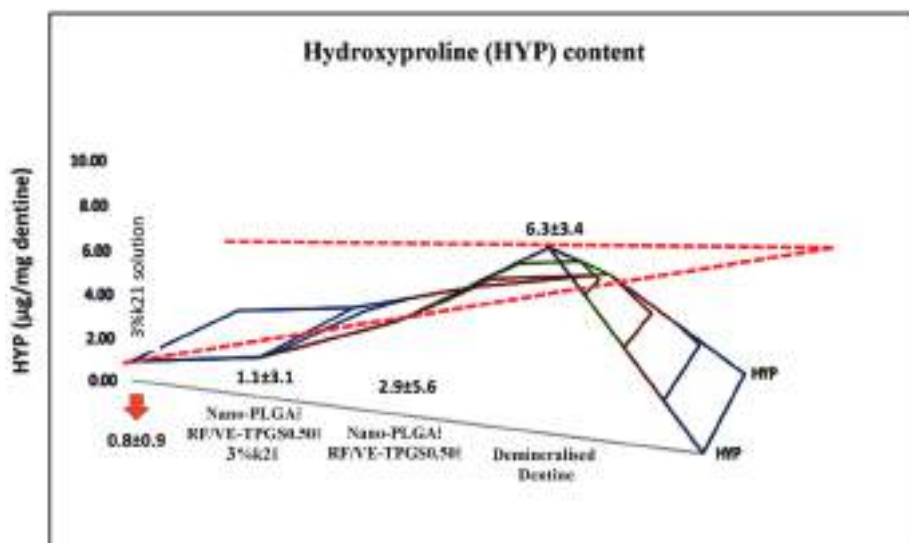


Fig. 6. Hydroxyproline (HYP) release from solubilized collagen peptide fragments in incubation medium for 24 h. Values are µg HYP/mg as values are means with \pm SD (n = 10).

nano-PLGA:RF/VE-TPGS_{0.50}:k21 against *S. mutans* has been evaluated by four different methods using blank and polymer drug ratios 1% and 2%. Bacterial species produce exopolysaccharides which play an important role in initial adhesion to host cells and development of an intricate biofilm architecture. Nanoparticles adhere and penetrate biofilm cells depending on their morphological and surface properties [47]. Nano-PLGA:RF/VE-TPGS_{0.50}:k21 have not only reduced the biofilm biomass (Table 2) but also minimized EPS production (Table 2). Moreover, nanoparticles have facilitated the separation of biofilms from surfaces as indicated by the detachment assay (Table 2).

Nano-PLGA:RF/VE-TPGS_{0.50}:k21 were suspended in water (1.37%) and applied to demineralized dentine-substrates in dropwise manner, micro-brush rubbed for 5s, gently air blown and dried by a wet cotton pellet which enhanced tubular penetration and retention (Fig. 3a–c), thereby preventing them from settling on the exposed dentin surfaces which could lead to adverse effect on resin-dentin bonded interface and strength. The two-step E&R dentin adhesive further guaranteed deep nanoparticle infiltration forming an intact hybrid-layer (Fig. 3d) and well-formed long resin tags that established a morphological association with nanoparticles (Fig. 3e and f). It is noteworthy to mention that in a clinical situation; dentine related parameters may vary. Here, coronal dentine was used for infiltration purposes. However, variation stemming from dentine histology could contribute to an infiltration difference demanding further attention in relation to potential clinical application [48]. Moreover, a simulated pulpal-pressure value of 20 cm H₂O used in accordance with previous studies, is only an arbitrary value and may attain negative range in some cases [49,50]. Such effects on nanoparticle infiltration should be considered under scrutiny. In addition, we etched dentine with phosphoric acid to remove smear layer and reveal wide dentinal tubules along with two-step adhesive systems as a routine established protocol in adhesive dentistry. It is still unclear if nanoparticle delivery would be affected by using other adhesive systems currently available in the market such as self-etch. Release of k21 from nano-PLGA:RF/VE-TPGS_{0.50}:k21 after tubular delivery and bonding resins infiltration should also be evaluated as it plays a crucial role in adapting conclusions based on the effect of delivery of nanoparticles. The N- and C-termini-axially telopeptide domains undergo contraction as a result of the RF/VE-TPGS formulation. This results in an improvement of collagen density leading to changes happening in the orientation of the tropocollagen molecules. This happens relatively due to the confirmation of the axial helical terminus along the long axis of the fibril within the secondary and tertiary-structure of collagen. The tocopherol compound also promotes conformational changes with a sealed hydrophobic component [51] attaching itself to the collagen fragment [52] maintaining the structured helical structure. There is a scavenging effect of the Vitamin E molecule on superoxides stabilizing the collagen membranes, indicative of its pivotal importance [53]. The unique VE-TPGS formulation penetrates comprehensively within the dentine [25,42] in the presence of dentine and dentinal fluid acting as oxygen and peroxide reservoirs [54]. These reservoirs are present on the collagen surface, eventually resulting in neutralization of free oxygen inside dentine which is present due to riboflavin free radical production. d-Alpha-tocopheryl-poly (ethylene-glycol) is responsible for improved penetration of riboflavin inside the collagen and subsequent crosslinking as there is RF accumulation by dentine collagenous based protein [55]. However, UVA absorption is shielded by riboflavin and may have limited penetration within extracellular matrices [56]. The formulation has the ability to improve structural integrity and conformational stability of dentine collagen fibrils. The improvement in collagenase-mediated resistance to degradation maybe attributed to higher uptake of RF by dentine collagen due to the presence of d-Alpha-tocopheryl-poly (ethylene-glycol). After micro-Raman band profiling, there were variations observed at 785 cm⁻¹ and 1450 cm⁻¹. Peaks assigned to ring breathing modes of DNA/RNA bases and to the deformation of C–H functional groups in lipids and carbohydrates, indicating that the treatment of these nanoparticles might damage or

disrupt nucleic acids and lower the carbohydrates inside the biofilm, rendering damage to developed biofilms. The low intensity of this carbohydrate-associated Raman peak suggested the damage or disruption of biofilm structures was evident. The compound k21 resulted in a direct alignment of MMP-2 and -9 using molecular docking studies with collagen (PDB ID: 1Q7D) and binding pocket with SiteScore (0.91599) and DScore (1.067736).

However, the overall crucial part of this study was to indirectly investigate the effect of released k21 from the nanoparticles. The profound antibiofilm effect reported with resin-dentine specimens modified with nano-PLGA:RF/VE-TPGS_{0.50}:3%k21 (Fig. 3) indicates the ability and efficiency of the released k21 from nanoparticles delivered to dentinal tubules followed by bonding-resins application to achieve the desired effect. The positive effect on the bond strength may also be attributed to the presence of bridged organosiloxane groups in the molecular backbone of k21 which shows great affinity to resinous adhesive [57]. It should be clarified that, nano-PLGA:RF/VE-TPGS_{0.50}:k21 having 3% k21 was selected for dentine infiltration studies compromise between having profound antibacterial/antibiofilm potential, physico-chemical characteristics, k21 release and acceptable cytotoxicity based on our *in vitro* investigation (Figs. 2 and 3) and (Tables 1 and 2).

5. Conclusion

Demineralized dentine-substrates modified with biodegradable nano-PLGA:RF/VE-TPGS_{0.50}:k21 exhibited superior antibacterial/antibiofilm effects against cariogenic *S. mutans* biofilms after bonding-resins infiltration without adversely affecting resin-dentine bond strength.

Acknowledgment & Competing Interests Disclosure

This work was supported, in part, by grant PG10402012 UWA Dental School and National University Health System (NUHS), Singapore, Oral Health Seed Grant R221000078733 and International Medical University [425/2018]. The authors report no conflicts of interest in this work, or relevant affiliations or financial involvement with any organization or entity with a financial interest in or financial conflict. No writing assistance was utilized in the production of this manuscript.

References

- [1] Berger D, Rakhamimova A, Pollack A, Loewy Z. Oral biofilms: development, control, and analysis. *High-throughput* 2018;7:24.
- [2] Busscher H, Rinastiti M, Siswomihardjo W, Van der Mei H. Biofilm formation on dental restorative and implant materials. *J Dent Res* 2010;89:657–65.
- [3] Kim DH, Kwon T-Y. *In vitro* study of *Streptococcus mutans* adhesion on composite resin coated with three surface sealants. *Restor Dent Endod* 2017;42:39–47.
- [4] Bürgers R, Cariaga T, Müller R. Effects of aging on surface properties and adhesion of *Streptococcus mutans* on various fissure sealants. *Clin Oral Invest* 2009;13:419–26.
- [5] Neu TR, Swerhone GDW, Lawrence JR. Assessment of lectin-binding analysis for *in situ* detection of glycoconjugates in biofilm systems. *Micro* 2001;147(Pt 2):299–313.
- [6] Pinna R, Maioli M, Eramo S, Mura I, Milia E. Carious affected dentine: its behaviour in adhesive bonding. *Aust Dent J* 2015;60:276–93.
- [7] Liu Y, Tjäderhane L, Breschi L, Mazzoni A, Li N, Mao J. Limitations in bonding to dentin and experimental strategies to prevent bond degradation. *J Dent Res* 2011;90:953–68.
- [8] Daood D, Yiu CKY, Burrow MF. Effect of a novel quaternary ammonium silane cavity disinfectant on cariogenic biofilm formation. *Clin Oral Invest* 2020;24:649–61.
- [9] Daood U, Yiu CK, Burrow MF, Niu LN, Tay FR. Effect of a novel quaternary ammonium silane on dentin protease activities. *J Dent* 2017;58:19–27.
- [10] Daood D, Yiu CKY, Burrow MF, Niu LN, Tay FR. Effect of a novel quaternary ammonium silane cavity disinfectant on durability of resin-dentine bond. *J Dent* 2017;60:77–86.
- [11] Ahlström B, Thompson RA, Edebo L. The effect of hydrocarbon chain length, pH, and temperature on the binding and bactericidal effect of amphiphilic betaine esters on *Salmonella typhimurium*. *APMIS* 1999;107:318–24.
- [12] Yuen John WM, Yung Jolene YK. Medical implications of antimicrobial coating polymers-organosilicon quaternary ammonium chloride. *Mod Chem Appl* 2013;1:3.

- [13] Daood U, Parolia A, Elkezza A, Yiu CK, Abbott P, Matinlinna JP, Fawzy AS. An in vitro study of a novel quaternary ammonium silane endodontic irrigant. *Dent Mater* 2019;35:1264–78.
- [14] Liu R, Xu Y, Wu D, Sun Y, Gao H, Yuan H. Comparative study on the hydrolysis kinetics of substituted ethoxysilanes by liquid-state ²⁹Si NMR. *J Non-Cryst Solids* 2004;343:61–70.
- [15] Xu Y, Wang Q, Feng Y. Enhanced oral bioavailability of [6]-Gingerol-SMEDDS: preparation, in vitro and in vivo evaluation. *J Funct Foods* 2016;27:703–10.
- [16] Uthumpa C, Indranupakorn R, Asasutjarit R. Development of nanoemulsion formulations of ginger extract. *Adv Mater Res* 2013;684:12–5.
- [17] Pandey A, Jain DS, Chakraborty S. Poly Lactic-Co-Glycolic Acid (PLGA) copolymer and its pharmaceutical application. *Handb Polym Pharm Technol* 2015;2:151–72.
- [18] Dalpiaz A, Sacchetti F, Baldisserotto A, Pavan B, Maretti E, Iannucelli V. Application of the “in-oil nanoprecipitation” method in the encapsulation of hydrophilic drugs in PLGA nanoparticles. *J Drug Deliv Sci Technol* 2016;32:283–90.
- [19] Silva A TCR, Cardoso BCO, Silva ESR, Freitas RFS, Sousa RG. Synthesis, characterization, and study of PLGA copolymer in vitro degradation. *J Biomaterials Nanobiotechnol* 2015;6:8–19.
- [20] Fawzy AS, Priyadarshini B, Selvan S, Lu TB, Neo J. Proanthocyanidins-loaded nanoparticles enhance dentin degradation resistance. *J Dent Res* 2017;96:780–9.
- [21] Tjäderhane L, Nascimento FD, Breschi L, Mazzoni A, Tersariol IL, Geraldini V. Optimizing dentin bond durability: control of collagen degradation by matrix metalloproteinases and cysteine cathepsins. *Dent Mater* 2013;29:116–35.
- [22] Yang B, Adelung R, Ludwig K, Bossmann K, Pashley DH, Kern M. Effect of structural change of collagen fibrils on the durability of dentin bonding. *Biomaterials* 2005;26:5021–31.
- [23] Sano H, Takatsu T, Ciucchi B, Horner JA, Matthews WG, Pashley DH. Nanoleakage leakage within the hybrid layer. *Operat Dent* 1995;20:18–25.
- [24] Zhang Z, Mutluay M, Tzvergill-Mutluay A, Tay FR, Pashley DH, Arola D. Effects of EDC crosslinking on the stiffness of dentin hybrid layers evaluated by nanoDMA over time. *Dent Mater* 2017;33:904–14.
- [25] Daood U, Matinlinna JP, Fawzy AS. Synergistic effects of VE-TPGS and riboflavin in crosslinking of dentine. *Dent Mater* 2019;35:356–67.
- [26] Osracolo C, Caruso C, Tronino D, Troisi S, Laneri S, Pacente L. Enhancement of corneal permeation of riboflavin-5-phosphate through vitamin E TPGS: a promising approach in corneal trans-epithelial cross linking treatment. *Int J Pharm* 2013;440:148–53.
- [27] Constantinides PP, Han J, Davis SS. Advances in the use of tocals as drug delivery vehicles. *Pharm Res (N Y)* 2006;23:243–55.
- [28] Meera Priyadarshini Balasankar, Mitali Kakran, Lu Thong Beng, Harish K Handral, Dubey Nileshkumar, Amr S Fawzy. PLGA nanoparticles as chlorhexidine-delivery carrier to resin-dentin adhesive interface. *Dent Mater* 2017;33:830–46.
- [29] Abd El-Hay AM, Naser AM, Badawi A, Abd El-Ghaffar MA, Abd El-Wahab H, Helal Doaa A. Biodegradable polymeric microcapsules for sustained release of riboflavin. *Int J Biol Macromol* 2016;92:708–14.
- [30] Kim HS, Park HD. Ginger extract inhibits biofilm formation by *Pseudomonas aeruginosa* PA14. *PLoS One* 2013;8:e76106.
- [31] Priyadarshini B, Selvan S, Narayanan K, Fawzy A. Characterization of chlorhexidine-loaded calcium-hydroxide microparticles as a potential dental pulp-capping material. *Bioengineering* 2017;4:59.
- [32] Priyadarshini B, Selvan S, Lu T, Xie H, Neo J, Fawzy AS. Chlorhexidine nanocapsule drug delivery approach to the resin-dentin interface. *J Dent Res* 2016;95:1065–72.
- [33] Daood U, Yiu CKY. Transdental cytotoxicity and macrophage phenotype of a novel quaternary ammonium silane cavity disinfectant. *Dent Mater* 2019;35:206–16.
- [34] Priyadarshini BM, Antipina MN, Fawzy AS. Formulation and characterisation of poly (lactic-co-glycolic acid) encapsulated clove oil nanoparticles for dental applications. *IET Nanobiotechnol* 2017;12:311–7.
- [35] Kumari A, Singla R, Guliani A, Yadav SK. Nanoencapsulation for drug delivery. *EXCLI J* 2014;13:265–86.
- [36] Priyadarshini B, Selvan S, Lu T, Xie H, Neo J, Fawzy AS. Chlorhexidine nanocapsule drug delivery approach to the resin-dentin interface. *J Dent Res* 2016;95:1065–72.
- [37] Misra R, Acharya S, Dilnawaz F, Sahoo SK. Sustained antibacterial activity of doxycycline-loaded poly (D, L-lactide-co-glycolide) and poly (ε-caprolactone) nanoparticles. *Nanomedicine* 2009;4:519–30.
- [38] Li J, Su L, Li J. Influence of sucrose on the stability of W1/O/W2 double emulsion droplets. *RSC Adv* 2015;5:83089–95.
- [39] Jacobs C, Müller RH. Production and characterization of a budesonide nanosuspension for pulmonary administration. *Pharm Res (N Y)* 2002;19:189–94.
- [40] Mainardes RM, Evangelista RC. PLGA nanoparticles containing praziquantel: effect of formulation variables on size distribution. *Int J Pharm* 2005;290:137–44.
- [41] Scheffel DL, Soares DG, Basso FG, de Souza Costa CA, Pashley DH, Hebling J. Transdental cytotoxicity of glutaraldehyde on odontoblast-like cells. *J Dent* 2015;43:997–1006.
- [42] Daood U, Sauro S, Rao MP, Omar H, Lin SL, Fawzy AS. Novel riboflavin/VE-TPGS modified universal dentine adhesive with superior dentine bond strength and self-crosslinking potential. *Dent Mater* 2020;3:145–56.
- [43] Lung CYK, Matinlinna JP. Silanes for adhesion promotion and surface modification. In: Moriguchi K, Utagawa SS, editors. *Silane, chemistry, applications and performance*. New York: Nova Science Publishers; 2013. p. 87–110.
- [44] Hosaka K, Nishitani Y, Tagami J, Yoshiyama M, Brackett WW, Agee KA. Durability of resin-dentin bonds to water- vs ethanol-saturated dentin. *J Dent Res* 2009;88:146–51.
- [45] Sadek FT, Castellán CS, Braga RR, Mai S, Tjäderhane L, Pashley DH. One-year stability of resin-dentin bonds created with a hydrophobic ethanol-wet bonding technique. *Dent Mater* 2010;26:380–6.
- [46] Mo SS, Bao W, Lai GY, Wang J, Li MY. The microfloral analysis of secondary caries biofilm around Class I and Class II composite and amalgam fillings. *BMC Infect Dis* 2010;10:241.
- [47] Wang T, Bai J, Jiang X, Nienhaus GU. Cellular uptake of nanoparticles by membrane penetration: a study combining confocal microscopy with FTIR spectroelectrochemistry. *ACS Nano* 2012;6:1251–9.
- [48] Mjör I, Nordahl I. The density and branching of dentinal tubules in human teeth. *Arch Oral Biol* 1996;41:401–12.
- [49] Berggreen E, Bletska A, Heyeraas KJ. Circulation in normal and inflamed dental pulp. *Endod Top* 2007;17:2–11.
- [50] Abd AE, Yu DC. Dental pulp neurophysiology: part 1. Clinical and diagnostic implications. *J Can Dent Assoc (Tor)* 2009;75:55–9.
- [51] Meier R, Tomizaki T, Schulze-Briese C, Baumann U, Stocker A. The molecular basis of vitamin E retention: structure of human alpha-tocopherol transfer protein. *J Mol Biol* 2003;3:725–34.
- [52] Cole DJ, Payne MC, Ciacchib LC. Water structuring and collagen adsorption at hydrophilic and hydrophobic silicon surfaces. *Physiol Chem Phys* 2009;11:11395–9.
- [53] Fariss M, Pascoe G, Reed N. Vitamin E. Reversal of the effect of extracellular calcium on chemically induced toxicity in hepatocytes. *Sci Asia* 1985;227:751–3.
- [54] Titley KC, Torneck CD, Ruse ND, Kmec D. Adhesion of a resin composite to bleached and unbleached human enamel. *J Endod* 1993;19:112–5.
- [55] Hayes S, Kamma-Lorger CS, Boote C. The effect of riboflavin/UVA collagen cross-linking therapy on the structure and hydrodynamic behaviour of the ungulate and rabbit corneal stroma. *PLoS One* 2013;8:e52860.
- [56] Hass V, Luque-Martinez IV, Gutierrez MF, Moreira CG, Gotti VB, Feitosa VP. Collagen cross-linkers on dentin bonding: stability of the adhesive interfaces, degree of conversion of the adhesive, cytotoxicity and in situ MMP inhibition. *Dent Mater* 2016;32:732–41.
- [57] Lung CKY, Matinlinna JP. Resin bonding to silicized zirconia with two and cross-linking silane, part I: experimental. *Siliconindia* 2010;2:153–61.